energies

Article

Identifying Harmonic Sources by Profiling Discrete Harmonic Cycle Time

Tommy Hjertberg * and Sarah K. Rönnberg

Electric Power Engineering, Department of Engineering Sciences and Mathematics, Luleå University of Technology, 931 87 Skellefteå, Sweden; sarah.ronnberg@ltu.se
* Correspondence: tommy.hjertberg@ltu.se; Tel.: +46-910-585380

Abstract: Harmonic emissions cause power quality issues in electrical systems, making source identification necessary to determine the best way of remedying them. Existing methods rely on measuring variations in harmonic amplitude, angle, and phase which require multiple measurement points or extensive system knowledge. We identified a methodological research gap because Discrete Harmonic Cycle Time (DHCT) has not been evaluated as a measuring principle for harmonic source identification. We propose a method using DHCT to enable single point measurements to profile harmonic sources. To determine the cycle length, we used a combination of sifting, a filter bank of cascaded high-pass and notch filters, and zero-crossing detection. For comparing the devices, we extracted motifs from the time series of discrete cycle lengths and applied principal component analysis. While it has previously been known in other contexts that harmonics can have varying cycle lengths, our laboratory results show that this is also true for the emissions of power electronic devices and that the differentiation can be used to identify the devices, thus bridging this knowledge gap. This method is independent of system impedance and topology. While further validation in more complex environments is needed, our results suggest that devices can be identified using this measurement principle. Since the measuring principle is orthogonal to other methods, it has potential as a complementary tool in harmonic source identification.

Keywords: Discrete Harmonic Cycle Times; harmonic source identification; harmonics; profiling; DHCT

check for updates

Academic Editor: Michael Negnevitsky

Received: 5 December 2024
Revised: 8 February 2025
Accepted: 9 February 2025
Published: 12 February 2025

Citation: Hjertberg, T.; Rönnberg, S.K. Identifying Harmonic Sources by Profiling Discrete Harmonic Cycle Time. *Energies* **2025**, *18*, 853. https://doi.org/10.3390/en18040853

Copyright: © 2025 by the authors. Licensee MDPI, Basel, Switzerland. This article is an open access article distributed under the terms and conditions of the Creative Commons Attribution (CC BY) license (https://creativecommons.org/licenses/by/4.0/).

1. Introduction

Waveform distortion caused by power system harmonics is an increasing problem with the growing use of power electronic components. Identifying which device is causing a distortion can be difficult, and several attempts have been made to solve this issue. We have found a methodological research gap since the potential of using Discrete Harmonic Cycle Time (DHCT) has not been previously investigated. Similar methods have been proposed previously in various applications such as recognising speech in the presence of background music [1], to identify types of stars by measuring the cycle time differences in their radial velocity in astrophysics [2], and for determining the time of a recording by the frequency of the electrical background hum in forensic technology [3]. To our knowledge, no similar method has been applied to the study of power system harmonics. So, our aim is also to investigate the knowledge gap that exists with regard to whether Discrete Harmonic Cycle Time varies between devices in a way that makes it possible to identify the devices. Harmonic power flow aims to determine which device is contributing the most to

a distortion by determining the active or reactive power flow at harmonic frequencies. The voltage–current ratio method attempts to draw conclusions by comparing the ratio between voltage and current as the Point of Common Coupling (PCC) to determine how much distortion a consumer is contributing [4]. Many metering devices can be placed and used to compare the measured amplitudes to the estimated ones with a Kalman filter in order to determine which source deviates from the estimate [5]. Harmonic Source Estimation is another approach that uses harmonic power flow and creates estimates for the harmonic levels in every point of a system. It uses deviations from these levels to locate sources of additional harmonic emissions, but combining the current metering required for the harmonic power flow with a demand for many measuring points is a drawback of the method [6]. We propose a method that is orthogonal to these approaches, and which only requires measurements of either voltage or current for determining the source of a harmonic distortion by examining small variations in the oscillation pattern of harmonic components emitted by power electronic devices.

We propose that power electronic devices can be identified by analysing the cycle length of harmonic emissions, which have an on-average constant frequency, but which has recurring variations in the length of individual cycles of the harmonic centre frequency. IEC defines the harmonic order as "The integral number given by the ratio of the frequency of a harmonic to the fundamental frequency" [7], while the fundamental itself is defined as "The component of order 1 of the Fourier series of a periodic quantity" [7]. IEC [8] indicates that when measuring harmonics, the fundamental should be taken as the power system frequency, and the Fourier transform should be made over ten fundamental cycles in a 50 Hz power system. This means that the measuring window is approximated to 200 ms, resulting in a frequency resolution of 5 Hz. Our proposed approach is related to the concept of instantaneous frequency as described by [9]. Instead of trying to establish a continuously defined phase angle, unwrapping and integrating it to obtain the instantaneous frequency of the signal, we take a different approach. We use the length of each cycle, which we refer to as the Discrete Harmonic Cycle Time (DHCT). This allows us to create a time series whose amplitude is given by the cycle lengths of a selected harmonic. Huang [10] proposed that statistical methods in combination with the Generalised-Zero Crossing (GZC) method could be used to analyse the intrinsic modes isolated by empirical mode decomposition. While GZC can detect quarter cycles, we propose using full cycle lengths to reduce random noise. Using a full cycle is equivalent to averaging over the quarter cycles, reducing the noise level by a factor of four. Instead of statistical methods, we employ data mining, specifically matrix profiling, to extract the relevant features and use these for signal comparison.

Fabus et al. [11] have proposed a stricter definition of harmonics than the IEC, where only sinusoidally driven oscillations would be considered as opposed to non-sinusoidally driven independent oscillations. They consider the problem in the context of electrocardiograms, where the spurious signals would presumably be injected by electromagnetic radiation. In contrast, we consider voltage and current harmonics in the power system where the root cause of variations is distortions of the current waveform caused by switching in the power electronic devices. We note that this is an observation of the same phenomenon as we investigate in this study: minute variations in the discrete cycle time at harmonic frequencies. The authors of [5] aimed to exclude harmonics originating from power electronic components using the characteristic variations they produce in the cycle length. In contrast, we strive to use these variations to identify what power-electronic components are causing them.

Empirical mode decomposition (EMD), as described by [9], is a method for isolating a time domain signal that consists of one specific oscillatory mode from a signal where many such modes are present through iterative sifting in the time domain. While this method

would seem like an obvious way to isolate the time domain waveform of the harmonics, it is not typically possible to separate frequency peaks that are closely spaced in the frequency domain, leading to mode mixing where the components blend. Our approach to solving this problem is first to isolate the harmonic using a combination of filtering and smoothing techniques and then apply sifting to extract only one waveform, which conforms to the requirements that [12] specifies for calling it an Intrinsic Mode Function. The Methods section of this paper describes the filtering and sifting process.

We similarly isolate the time domain expression of the oscillatory pattern of a power system harmonic. However, since we are examining the properties of a component with a known and well-defined central frequency, it is unnecessary to iteratively subtract the intrinsic modes in the time domain to discover it as in traditional EMD. Instead, we apply a high-pass filter to eliminate the fundamental, cascaded with notch filters to eliminate the other harmonics and modified Savitzky–Golay smoothing to eliminate the high-order noise. Sifting is used as a final means to eliminate the low-frequency distortion that the high-pass filter did not remove.

Fingerprinting techniques are being actively developed in the field of computer security, where they can be used to identify devices and software and even track individual users. The use of temporal packet data to identify network devices has been proposed by [13] and while the mechanisms behind harmonic emissions and data packet generation are unrelated, using temporal features to create a fingerprint is similar to what we are trying to accomplish in harmonic source identification. Similarly to how they propose increasing fingerprint accuracy by gathering more features, DHCT is a further feature of harmonic sources that can be used in conjunction with other features to create a more distinctive fingerprint for devices or classes thereof.

In Section 2, we describe the method that was used from the laboratory setup through the filtering techniques and zero-crossing detection and, finally, the method used for comparing signals. Section 3 describes the results of the measurements and the comparison between the signals obtained from various devices in isolation as well as in combination with each other. Section 4 discusses the results, the challenges and the opportunities of DHCT. Section 5 draws some conclusions about the viability of the method and lays out some future works.

2. Materials and Methods

To precisely detect the discrete cycle time of a frequency component mixed in with many spurious frequency components, the waveform of that component must first be isolated. Such isolated waveforms of distinct signal components are referred to as Intrinsic Mode Functions (IMFs) by Huang et al. Their definition of an IMF is that the waveform has the same number of positive and negative peaks or that they differ at most by one and that there is precisely one zero crossing between each peak and trough [12]. The smoothness is crucial for correctly estimating the instantaneous frequency, but it is not as important when detecting discrete cycle length through zero-crossing detection. However, low-frequency components would cause the stretching and compressing of the discrete cycle times, and high-frequency components could cause rapid successive zero-crossings. Before using zero-crossing detection to determine the discrete cycle time, the signal was processed through filtering, smoothing and time domain sifting. Traditional band-pass filters work well when the signal features are clearly defined in the frequency domain. When investigating deviations around a central frequency, it is not straightforward to determine how they will manifest in the frequency domain. The methods described here are intended to act as a band-pass filter without distorting the underlying waveform. The

whole process from a measured signal to a signal of discrete cycle time is described by the flow chart in Figure 1 and the signal at different stages can be seen in Figure 2.

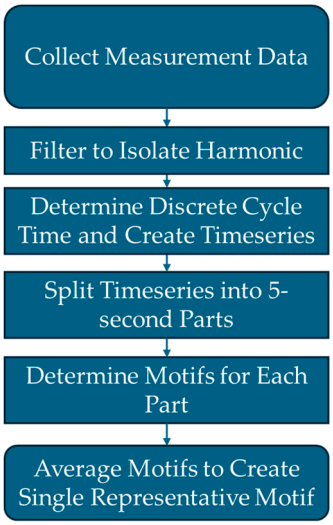


Figure 1. Flow chart of the process of extracting a representative motif using DHCT.

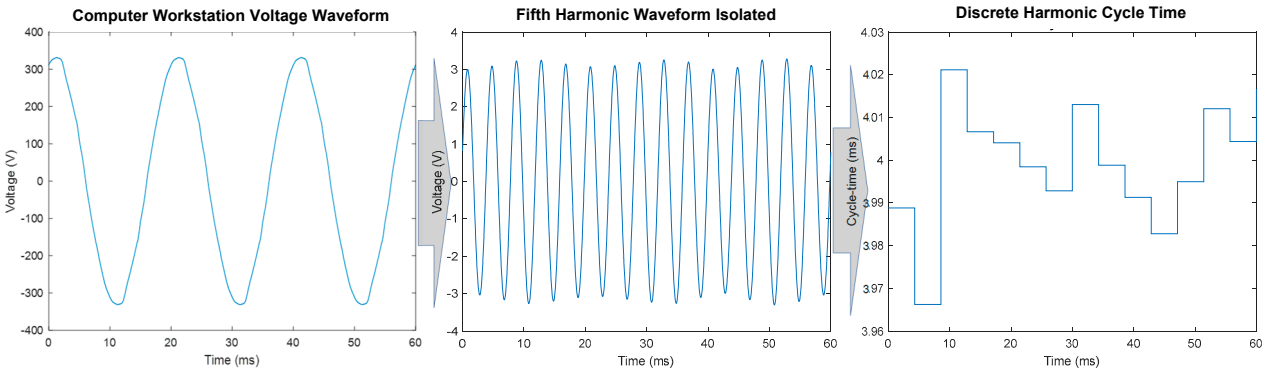


Figure 2. The process from signal to discrete cycle time.

2.1. Laboratory Measurements

The measurements were performed in a laboratory with power electronic devices connected to a Controllable Voltage Source (CVS). The current and voltage were measured using a high-speed data acquisition system, Dewesoft Sirius HS [14]. The sampling rate was set to 500 kHz with a 16-bit depth. The voltage was measured using the high-voltage input of the acquisition system with a range of ±400 V peak value. This means that the quantisation step is $\frac{800\ \mathrm{V}}{2^{16}} \approx 12$ mV, and the specified noise floor is −79 dB, or 9 mV. The voltage measurement was only used to determine the background spectrum of emissions from the CVS. The current was measured using a Pearson Electronics model 4100 C current monitor [15] connected to the low voltage input of the acquisition system, configured for a range of ±2 A. This means that the quantisation step is $\frac{4\ \mathrm{A}}{2^{16}} \approx 61\ \mu$A. With the current probe connected, but with no current flowing, the peak noise measured for 3 min was 306 μA. This can be considered as the noise floor and constitutes the limit of the accuracy of the current measurement. The laboratory setup is shown in Figure 3.

The CVS used was Chroma ATE's model 61505 [16] configured to output a 50 Hz sinewave at 230 V RMS with a source resistance of 0.4 Ω and a source reactance of 0.8 mH. Measuring the no-load emission produced the background voltage spectrum shown in Figure 4. The total harmonic distortion ($\mathrm{THD_V}$), computed according to [8], was 0.31%.

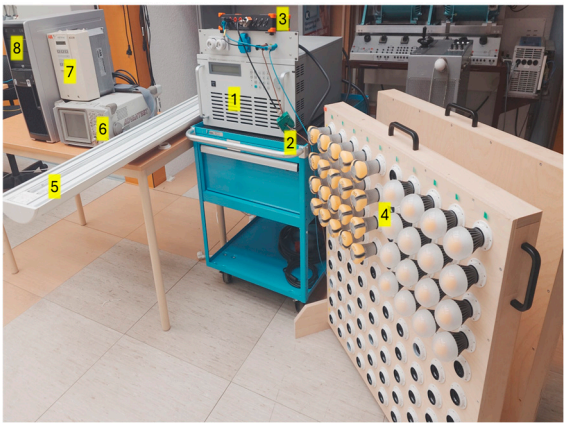


Figure 3. Overview of the devices used in this study: 1. controllable voltage supply; 2. current probe; 3. data acquisition system; 4. LED array; 5. fluorescent tube; 6. spectrum analyser; 7. variable frequency drive; 8. workstation. The devices were connected directly to the CVS and the current was measured using the current probe placed around the phase wire.

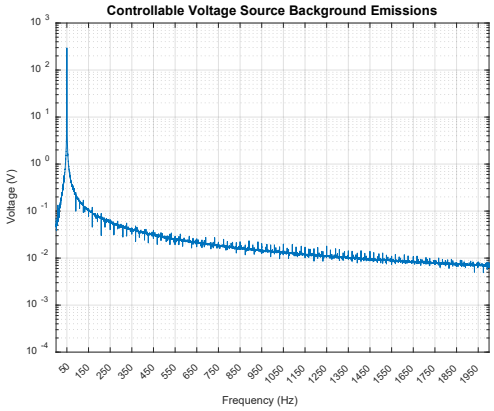


Figure 4. CVS no-load voltage spectrum, measured over 10 s.

While the harmonic distortion is very low for the CVS, the harmonic impedance also appears very low. This means that the harmonic voltages measured from the devices we connected were too low to separate from the background emissions and the noise. Empirically, we determined that an SNR of 40 dB after applying the cascaded filter was necessary for reliably applying the proposed method, which was not achievable when measuring the harmonic voltage using the CVS. Because of this, only current measurements were used for this paper.

2.2. Filtering

To make a time-domain analysis of a specific harmonic, it is necessary to isolate it from the fundamental and other harmonics, interharmonics and high-bandwidth noise. Using a too-narrow band-pass filter would destroy or distort the information in the signal about the discrete cycle time variations we are trying to study. Since most of the signal energy from other harmonics is contained in a narrow band around the centre frequency, we have used a filter bank consisting of cascaded notch filters to eliminate the unwanted harmonics. The IEC defines sidebands as the spectral components resulting from modulation above or below the carrier frequency [17]. Since the harmonics themselves are, in this sense, sidebands to the fundamental frequency, we use the term "spectral skirt" to describe the frequencies rolling off from the central frequency regardless of whether that central frequency is the fundamental or the harmonics. The fundamental has spectral skirts with a relatively high amplitude, so a high-pass filter with a cut-off frequency of 100 Hz was used

to remove the fundamental and most of its spectral skirt. The notch filters were limited to suppressing harmonics up to 1 kHz since the higher-order harmonics are usually lower in amplitude, and the smoothing will act as a low-pass filter. Since even order harmonics are generally not present, those are also omitted from the notch filter. A cascaded filter designed for 250 Hz is shown in Figure 5. Both the high-pass and the notch filters are second-order Butterworth filters.

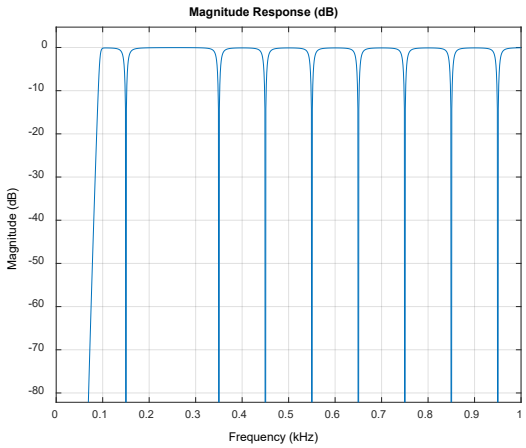


Figure 5. Response of the cascaded notch- and high-pass filters.

The filtering methods were chosen to preserve enough information about cycle-time variations without the noise and influence from the other harmonics imposing excessive distortion. Empirically, after filtering, a signal-to-noise ratio of 40 dB between the harmonic being studied and the noise, including higher-order harmonics, is required to extract the discrete cycle time variations.

2.3. Smoothing

A modified Savitzky–Golay (SG) filter was used to smooth the signal. The working principle of SG smoothing is that a polynomial of degree N is fitted using least-squares interpolation to M samples to either side of the sample being processed, and the value of the sample is then made into the value of the polynomial in that point. In its simplest form, with a polynomial of degree one, SG smoothing would be equivalent to a moving average with the squared distances as weights. SG smoothing does not have an exact definition in the frequency domain. Its frequency characteristics are determined partly by how well the polynomial fits the underlying signal. Nevertheless, [18] showed empirically that an approximate cut-off frequency f_c can be expressed by

$$f_c = \frac{N+1}{3.2M - 4.6} \frac{f_s}{2}, \tag{1}$$

where N is the degree of the filter and M is half the window length minus 1 (since the window of an SG smoother always extends an equal number of samples around the centre sample that is being estimated). f_s is the sampling frequency and it is divided by two to convert the equation from normalised frequency.

When viewed as a low-pass filter, a well-known drawback of SG smoothing is the low stop-band attenuation and high stop-band ripple. Ref. [19] showed that this can be alleviated by using a Modified Sinc (MS) instead of the usual polynomials, where the modification is the tapering of the Sinc at the beginning and the end to compensate for the ringing that is otherwise typical of SG when the signal changes abruptly. The frequency characteristics of SG and MS are not an explicit property but rather an emergent feature of the smoothing algorithm. We used a frequency sweep to verify their frequency domain

characteristics to ensure that the degree and kernel length chosen would not eliminate the frequency under study. Using Equation (2), a filter length of 2651 and a degree of 4 was determined to have a cut-off frequency of 318 Hz. Figure 6 shows the result of a frequency sweep from 0 to 1 kHz for both the standard SG smoother and the MS smoother proposed by [19]. Due to its superior stop-band performance and equivalent pass-band behaviour, the MS smoother was used throughout this work. For comparison, the frequency response of moving average smoothing with a length of 1000 samples was also included.

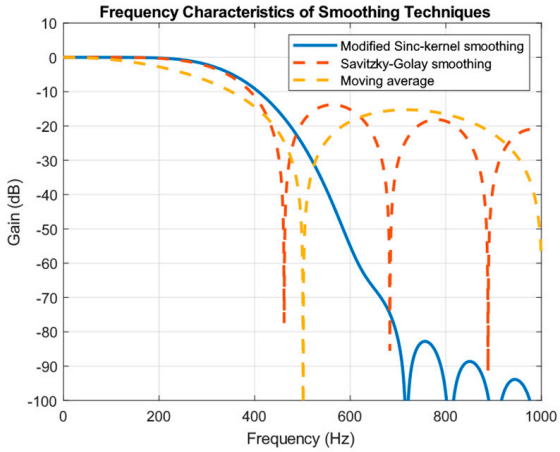


Figure 6. Frequency response of fourth-degree SG smoothing, Modified Sinc-smoothing and moving average smoothing.

2.4. Zero-Crossing Detection

The time difference between two consecutive positive flank zero-crossings of the filtered signal was used to measure cycle time. To avoid sampling distortion, Least-Square Polynomial Fitting was used as described by [20] to determine the zero points accurately. Two samples before and two samples after the zero crossing were used to create the polynomial. Figure 7 illustrates how the precision of the zero-crossing is improved with polynomial interpolation (shown in green) compared to the default method of MATLAB's zerocrossrate command [21]. More precisely, the sampling distortion of the basic method would be one whole timestep, resulting in an error bounded by

$$\varepsilon < \frac{t_s}{T}, \; for \; t_s < 2T \tag{2}$$

where T is the cycle time, t_s is the sample time and ε is the error coefficient. With polynomial fitting, the accuracy is not limited by the width of the timestep except in the sense that the machine precision could be interpreted as a timestep. While we do not have an analytic expression for the bounds of the error, a sweep through all possible angles for the points closest to the zero crossing with a resolution of 1 degree for each frequency up to the Nyquist frequency yields a maximum error coefficient, as shown in Figure 8. A closer look reveals that the error coefficient at 33% of the Nyquist frequency is less than 1‰, demonstrating that with this method, a sampling frequency of 450 kHz would be sufficient to estimate the cycle length up to 150 kHz with an error that is well below the measurement noise floor.

With a sampling rate of 500 kHz, the ninth harmonic is 0.18% of the Nyquist frequency, making the error coefficient smaller than 10^{-6}, as seen in Figure 8, which, multiplied by the step length, gives a margin of error of

$$\frac{10^{-6}}{500 \text{ kHz}} = 2 \text{ ps}, \tag{3}$$

which is a conservative margin in line with [20], who found that the margin of error before accounting for noise was two orders of magnitude smaller than this when using a 10 MHz sampling rate.

The criteria used for determining if cycle lengths have been extracted sufficiently well is that the average of the measured cycle lengths matches the expected value, for example, that the average of the ninth harmonic cycle lengths is $\frac{1}{450\ \text{Hz}} \approx 2.22$ ms with a permitted margin of error of ± 0.1 ms.

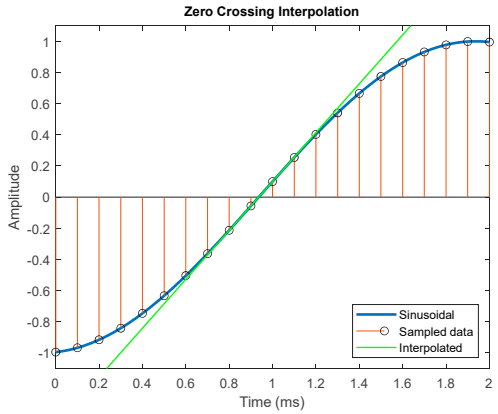


Figure 7. A sinusoidal signal sampled at 10 kHz, compared with the first-degree polynomial interpolation around the zero crossing.

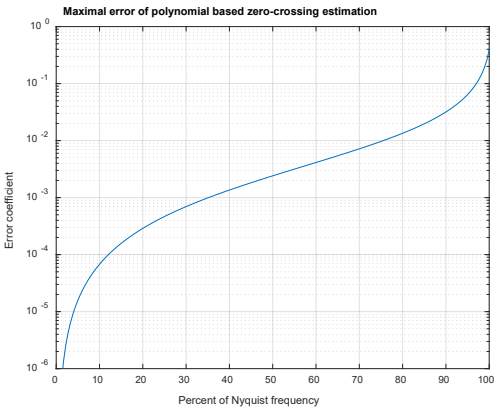


Figure 8. Maximum error in cycle length estimated by first-degree polynomial approximation of the zero crossing in a perfect sinusoid.

2.5. Comparing Signals

When comparing the time series, there are three main challenges: noise, transients and trends. Noise is any random distortion, and it can generally be compensated for by averaging, provided that the signal is stationary. The test we used for stationarity is that the autocorrelation functions were the same for all times. Figure 9 shows how the autocorrelation is almost perfectly stable over time, indicating that the signal is indeed stationary.

Transients are limited in time, and they do not recur regularly. Trends are long-term changes to the average of the signal, and in the context of harmonic cycle lengths, they are often the result of slow changes to the grid frequency. Some power electronic components might also have different operating modes, such as a converter driving an accelerating motor, which might behave differently from a converter driving a decelerating motor.

The variations in behaviour can be mitigated by splitting the measurements into shorter epochs. We have chosen to use epochs that are 5 s long. This has two benefits. The main benefit is that features can be averaged to reduce noise. But using shorter epochs

also means that there are more of them for a given measuring time, which means that any transients are likely to be isolated to a single epoch and can later be eliminated as outliers. Both sifting and smoothing suffer from edge effects at the beginning and end of the signal epoch and when the signal changes abruptly, so it would not be recommended to have epochs that are too short.

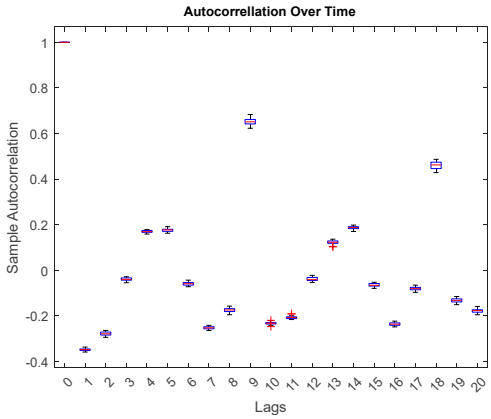


Figure 9. Boxplot of autocorrelation functions for discrete cycle time variations in the ninth harmonic of an LED array. The boxes represent 30 measurements, showing that the autocorrelation functions are stable over time.

A matrix profile is a method for comparing every part of a certain length of a signal to every other part of the signal. The principle is to select a feature length, slide along the time series, compare a window starting at each timestep to every other time, and compute a similarity score using the Euclidian distance after z-normalisation. We used the Interactive Matrix Profiler 3.0 [22] to extract the matrix profiles of our data. The segment with the lowest Euclidean distance to any of the other segments is selected as the first motif and further motifs can be selected and ranked based on their Euclidean distance to their Euclidean distances.

When studying the ninth harmonic, a feature length of 9 is appropriate since it covers one period of the fundamental frequency. There are methods for having a variable feature length, such as those demonstrated by [23], but if different measurements had different feature lengths, it would complicate making comparisons between signals. In practice, there is no need for methods to determine the feature length when there is an underlying known property, such as the fundamental period time that is confirmed by a strong autocorrelation at that lag. Examining the autocorrelation of our measurements when filtered for the ninth harmonic, we found that they have a strong 9-sample periodicity. If the frequency under study was subharmonic, such as the 16⅔ Hz frequency of the Swedish railway grid and its second harmonic relative to the main grids 50 Hz frequency, it might be necessary to use more advanced methods for selecting the feature length.

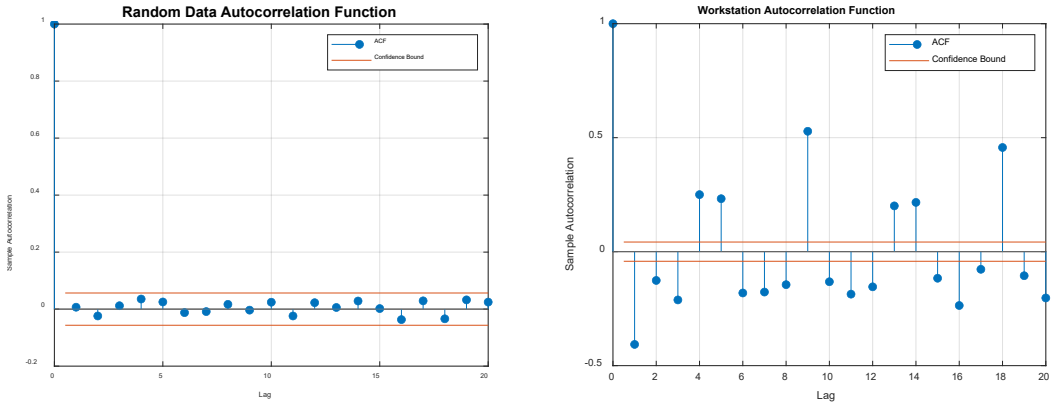
The Euclidean distance was used to quantify the difference between signals. Noise and transients could reduce the similarity, and trends could lead to a falsely high similarity. Since the measurements are asynchronous, transient distortions will not affect different measurement sets equally. To reduce the effects of intermittent or transient distortion, the samples being compared should be short but also representative. They must also contain enough information to represent the underlying process. To estimate a proper sample length, we use autocorrelation to determine the length of underlying structures in the signal. We have extracted the discrete cycle lengths and are now considering them as a signal where we are, again, determining the periodicity in the changes in discrete cycle times.

By using autocorrelation, we can accomplish two things simultaneously: determine the periodicity of the discrete cycle times and ensure that their variations are not random

processes. For a completely random process, the autocorrelation functions would tend to zero, but in practice, there needs to be a criterion for when the autocorrelation functions are small enough to be considered insignificant. The criterion typically used to decide whether an autocorrelation function is significant or not is the standard error SE computed as

$$SE = \sqrt{\frac{1}{N}\left(1 + 2\sum_{i=1}^{N-1} ACF^2(i)\right)} \tag{4}$$

where N is the number of samples and $\mathrm{ACF}(i)$ is the autocorrelation function at sample i [24]. This standard error implies that if the data are Gaussian random, 95.4% of the ACFs will have a lower magnitude than this. The ACFs of random data can be seen in Figure 10a, and the ACFs of discrete cycle times for a computer workstation can be seen in Figure 10b. While random data will, statistically in 4.6% of the cases, create ACFs with a higher autocorrelation than the confidence bound, an autocorrelation as strong as the one shown in Figure 10b would be exceedingly unlikely to be produced by random data.



(**a**) (**b**)

Figure 10. The 20 first autocorrelation functions of (**a**) random data and (**b**) the discrete cycle lengths of the ninth harmonic of a computer workstation.

While the negative correlation at the first lag in Figure 10b indicates that the data have an alternating pattern, it would be too little information to correlate segments of just two samples. When examining the cycle lengths of the ninth harmonic, the strongest autocorrelation is consistently at the ninth lag. This makes intuitive sense since it matches the fundamental frequency.

3. Results

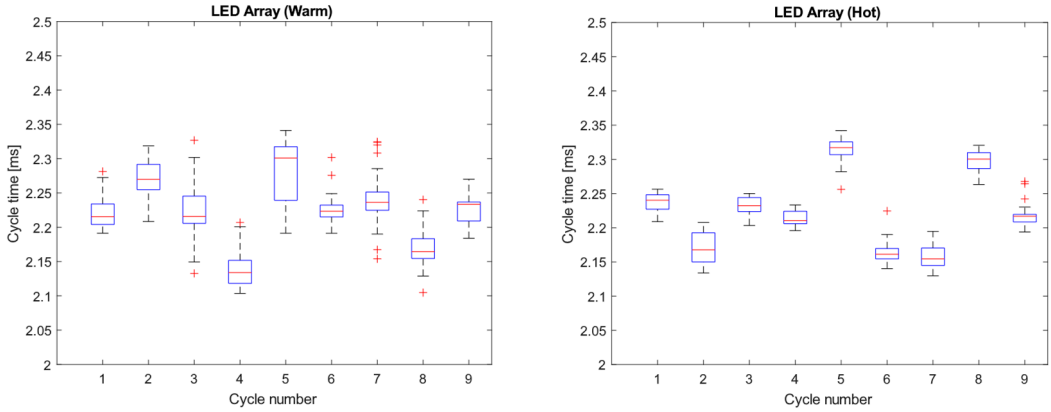
The discrete cycle length variation in the ninth harmonic was measured for various combinations of devices. The results are shown as boxplots in Sections 3.1 and 3.2, where each device is run for three minutes, resulting in 30 five-second samples for each of them. The boxplots represent the most similar motifs. Since the motifs are taken from periodic signal features, circle-shifting has been performed according to the best fit for Euclidean distance. The y-axis scale is consistent except for the Spectrum analyser, demonstrating a degenerated signal. The spectrum analyser's cycle length does not average to 2.22 ms, which all the other devices do, indicating that its pattern is the result of mode mixing. The fluorescent tube and the VFD also show a considerable variation in the cycle length, but they are the correct frequency on average. Table 1 indicates the average harmonic current magnitude of each device.

Table 1. Average amplitude of the ninth harmonic for each tested device.

Device	Ninth Harmonic Current Amplitude
Spectrum analyser	6.6 mA
LED array (after running > 30 min)	44 mA
LED array (after running >1 h)	23 mA
VFD	14 mA
Fluorescent tube	1.8 mA
Computer workstation	3.3 mA

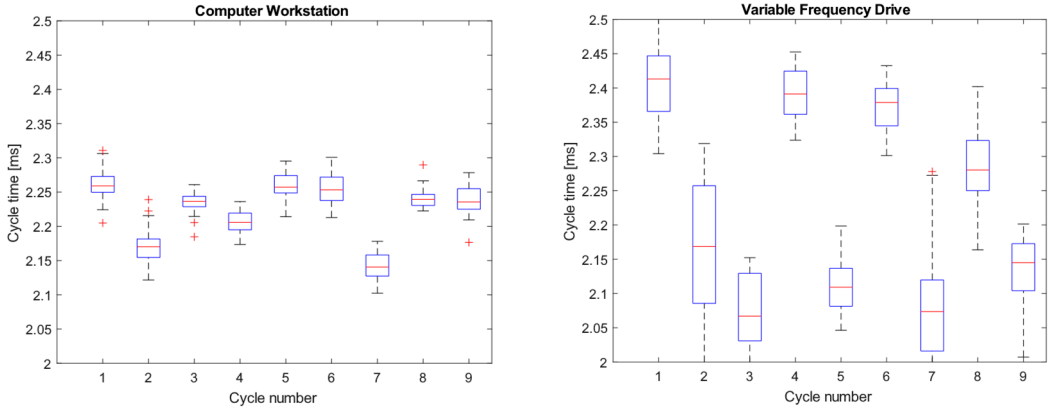
3.1. Device in Isolation

The discrete cycle time variations for different devices when they are connected on their own to the CVS are shown as boxplots in Figures 11–13. Since the data are cyclic, it is not possible to determine where in the cycle that the motif starts to be extracted, but they have been circularly shifted to where the Euclidean distance between them is the smallest. This was performed taking the first epochs motif as a reference and then cycling the others to where the Euclidean distance was the smallest with reference to it.



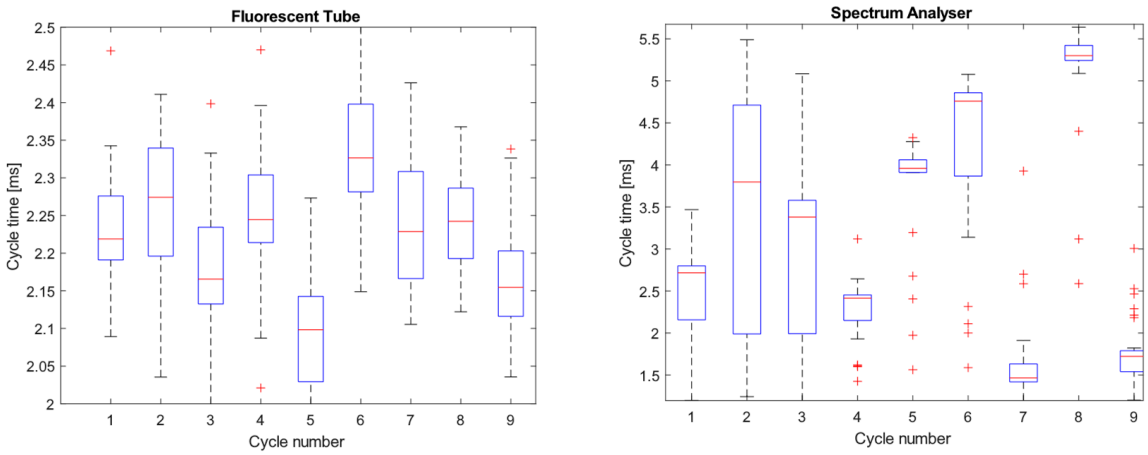
(**a**) (**b**)

Figure 11. Representative epochs of the discrete cycle time from 30 samples of the ninth harmonic of the LED array. Subfigure (**a**) shows the behaviour of the LED array after it has been turned on for just over 30 min and (**b**) shows how the LED array behaves after it has been turned on for more than 1 h.



(**a**) (**b**)

Figure 12. Representative epochs of the discrete cycle time from 30 samples of the ninth harmonic of (**a**) a computer workstation and (**b**) a VFD set to output 16.7 Hz (no load was connected to the VFD output).



(**a**) (**b**)

Figure 13. Discrete cycle time of the representative epochs from 30 samples of the ninth harmonic of (**a**) a fluorescent tube and (**b**) a spectrum analyser. Note that the vertical axis of the spectrum analyser boxplot is different from that of the other devices.

3.2. Combinations of Devices

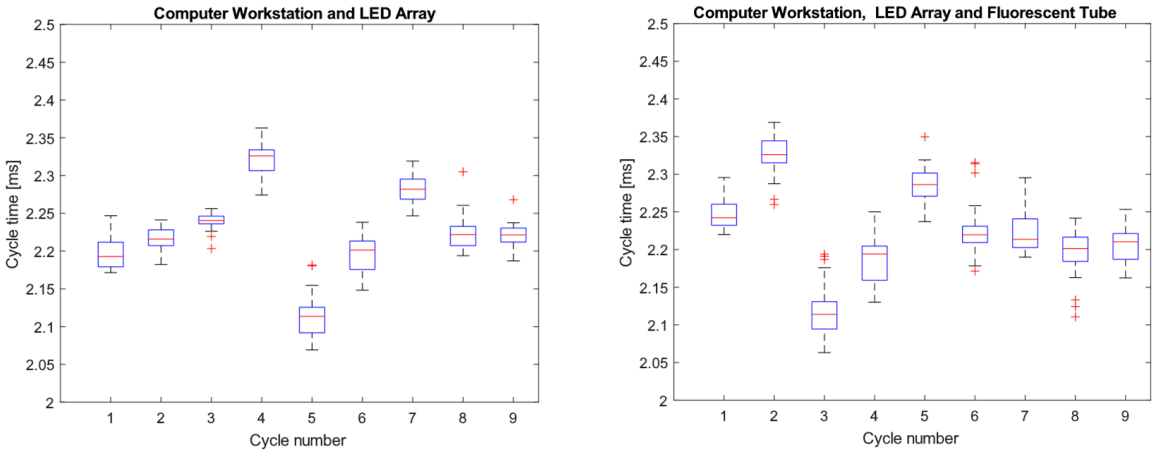
As was shown above, the output from the different device measurements are visually distinct. Figures 14 and 15 show how the output is affected when devices are combined. However, detecting if a measurement matches the original measurements of a device is challenging due to the varied characteristics of the motifs. We addressed this by computing the principal components for each device's measurements, projecting new measurements onto these components, and calculating the distance between the projections and the original measurements for each combination of devices. A match was considered as correct if it contained one of the devices included in the measurement as well as the measurement it was compared to. The 17 measurements are listed in Table 2. The resulting matches are listed in Table 3.

Table 2. Enumeration of measurements.

Nr	Device Combination	Nr	Device Combination
1	Workstation	10	LED array warm, tube light and spectrum analyser
2	Workstation and LED array	11	LED array hot (>1 h runtime)
3	Workstation, LED array and tube light	12	LED array hot and spectrum analyser
4	Workstation, LED array, tube light and spectrum analyser	13	Spectrum analyser
5	Workstation, VFD and spectrum analyser	14	Spectrum analyser and tube light
6	Workstation, VFD, spectrum analyser and LED array	15	VFD
7	Workstation, VFD, spectrum analyser, LED array and tube light	16	VFD and tube light
8	LED array warm (>30 min runtime)	17	Tube light
9	LED and tube light		

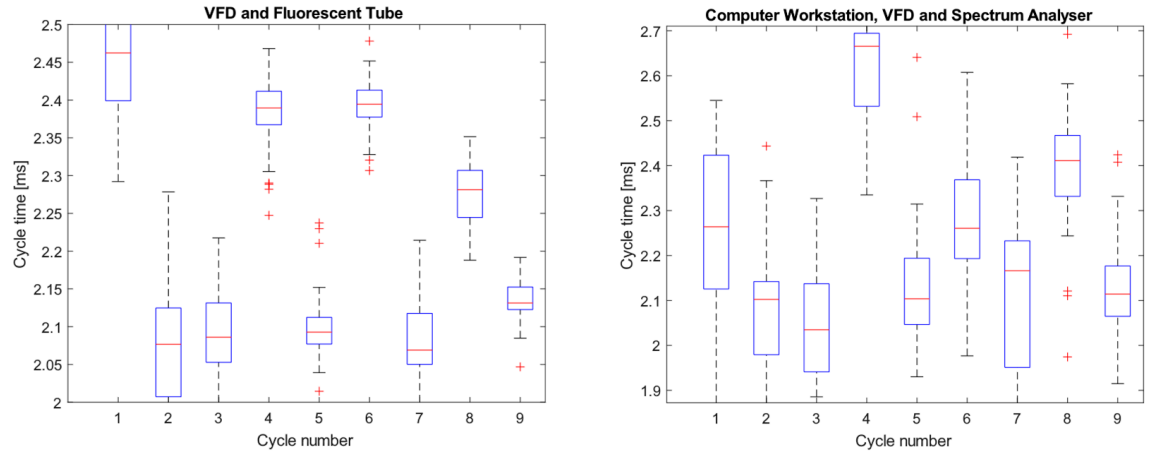
The results were compared to a Monte Carlo simulation of the same number of measurements. They were randomly combined in one million iterations to determine how likely it would be to obtain a certain number of correct matches by chance. With 14 correctly matched measurements out of 17, the probability of randomly reaching 14 correct matches is 0.034, with a margin of error of 0.001, according to the Monte Carlo simulation, indicating that the result is statistically significant. Since the LED array changed its profile after prolonged use, as was shown in Figure 11, it has been treated as two different devices. Measurement 9 is thus marked as incorrect since it was made before the LED array had

been left to warm up a second time. However, since the LED array had been used in several measurements before, it was likely in between these two temperature states. A total of 11 measurements were correctly matched with the device with the highest current draw. However, some of these measurements were of single devices matched to other measurements of the same device, which does not say anything about selectivity. Selecting the correct matchings, where there was more than one device, 6 out of 10 were correctly matched to the device with the highest harmonic current draw. The probability of randomly matching 6 out of 10 devices is 0.189 with a margin of error of 0.001, according to the Monte Carlo simulation, meaning that this result is not statistically significant. Based on measurements 6 and 7, it seems that there is a tendency for the spectrum analyser to dominate even though it has a lower amplitude.



(**a**) (**b**)

Figure 14. Discrete cycle time of the representative epochs from 30 samples of the ninth harmonic of (**a**) a combination of a computer workstation and an LED array and (**b**) the same combination but with an added fluorescent tube. In both of these cases, the LED array was warm, and the computer had completed its booting process.



(**a**) (**b**)

Figure 15. Discrete cycle time of the representative epochs from 30 samples of the ninth harmonic of (**a**) a combination of a VFD and a fluorescent tube and (**b**) a computer workstation, a VFD and a spectrum analyser. The VFD was outputting 16.7 Hz but had no load connected to it, the computer had finished booting and the spectrum analyser had completed its warmup process.

Table 3. List of matchups between measurements. Incorrect matches have a grey background. An asterisk marks the matches where the match is according to the device with the highest current draw. Measurement 9 has been marked with a slightly lighter grey since the LED array was likely somewhat heated by then.

Nr	Matching Nr	Nr	Matching nr	Nr	Matching Nr
1	1 *	7	13	13	13 *
2	9 *	8	8 *	14	14 *
3	9 *	9	11 *	15	15 *
4	15	10	16	16	16 *
5	15 *	11	11 *	17	16
6	13	12	16		

4. Discussion

The results support that discrete cycle lengths of harmonic emission from power electronic devices do vary between different devices, and this property can be used to identify a device that is present in a measurement. A drawback of this method is that devices with different operating modes can have different representative motifs. Figure 11 demonstrates this for the LED array, where the representative motifs have changed a bit from when the LED lamps had been turned on for 30 min as compared to when they had been turned on for hours. It should be noted that this is an expected behaviour of LED lamps. Reference [25] showed that the behaviour of LED lamps tend to stabilise after heating up for 40 min. This problem is not unique to this method but affects traditional fingerprinting techniques as well. This result indicates that the method could likely be improved with the help of machine learning techniques that could be used to learn the behaviour of different devices from the aspect of DHCT. The efficiency of using such techniques for classifying devices from the perspective of phase features was demonstrated by [26] and it seems likely that it would work equally well with DHCT.

The combination of a Modified Sinc smoother, a conservative high-pass and comb filter and time domain sifting to remove remaining low-frequency distortions was shown to work well for extracting the waveform of a specific harmonic so that the discrete cycle time can be detected. The computational complexity of so many steps is not entirely desirable, but since we were able to implement it in MATLAB, an interpreted language, it should be possible to run it at a much higher speed if implemented in a compiled language.

The measurements made with combinations of the spectrum analyser and other devices were visually quite chaotic. Table 3 shows the resulting matchings. Of the measurements that were incorrectly matched, numbers 4 and 12 contained the spectrum analyser. The spectrum analyser was present in 8 out of 17 measurements, so if it had a negative influence on the matching, that influence does not seem to be very strong.

The main result is that we could differentiate devices based on the discrete cycle time of one of their harmonics. This shows that the method could be useful for identifying harmonic-emitting devices. Another tentative result is that the devices' current draw likely impacts which measurements are matched. This suggests a capture effect, meaning that the device with the highest harmonic current drawn will dominate when several devices are connected. This effect was not statistically significant, but it indicates that the hypothesis might be correct and should be investigated further. There were some surprising results such as that of measurement 10, which had the LED array that drew a harmonic current of 44 mA and the tube light that drew 1.8 mA but was matched with the tube light and not the LED array. This might suggest that there are further mechanisms besides the magnitude of harmonic current drawn that affect which devices dominate the discrete cycle length.

The method that we implemented for this paper is quite computationally demanding, but this is a problem of implementation rather than a high time complexity. For this study,

it was implemented in MATLAB R2024a. Using a desktop computer equipped with an AMD Ryzen 3900X processor and 32 GB of memory, the processing time for the whole batch of measurements was around 12 h. The time complexity of EMD was shown by [27] to be $\mathcal{O} = N \cdot log(N)$; since applying FIR and IIR-filters is a set number of multiplications, it will have the complexity of $\mathcal{O} = N$, the Savitzky–Golay smoothing has a complexity of $\mathcal{O} = N$ since it is fundamentally an FIR filter [19], and the zero-crossing detection is an implementation of least squares-approximation so it could be implemented with a time complexity of $\mathcal{O} = N \cdot log(M)$ where M is the number of coefficients [28]. Since M is constant, the time complexity of the method above and including the extraction of the discrete cycle times will be $\mathcal{O} = N$. The extraction of the motifs was made using the SCAMP algorithm which has a time complexity of $\mathcal{O} = N$ but it should be noted that it is applied to the time series that is made up of cycle lengths, so it is applied to a much smaller number of samples than the previous steps. The final comparison step of using principal component analysis is applied only to the motifs, meaning that its time complexity can be neglected.

Since the time complexity is $\mathcal{O} = N$ the relevant question is the number of samples. It could be drastically reduced by reducing the original sampling rate since the zero-crossing detection used is robust with regard to sample rate. As shown in Figure 8, the error is below 0.1% up to 10% of the Nyquist frequency, and since this noise can be expected to be random, it will also be mitigated by the averaging process. Given that a sampling frequency of 10 times the measured harmonic would be used, a practically useful speed should be achievable, but since this study was made as a proof of concept, speeding up the implementation was not a priority.

This work has mainly focused on using DHCT for source identification, but another use for it could be to make long-term power quality studies where a harmonic is measured during an extended period of time and DHCT is used in combination with machine learning to determine which devices are producing certain amplitude patterns, similar to how [29] proposes using the load patterns to identify the power usage of consumer devices.

5. Conclusions

Our study shows that this method is applicable for discriminating between different harmonic sources, but it also indicates that it might suffer from some of the drawbacks that existing methods are affected by, such as not being invariant to changes in operating points. While this result is useful as a proof of concept, the method needs to be developed further to be a viable alternative for harmonic source identification in a practical setting.

Implementing this method requires much work to be usable in a practical setting. It would need to be implemented in a compiled language rather than MATLAB, and the sample rate should be optimised. The method for isolating the harmonic used here should be regarded as a proof of concept and a practical implementation could be made with other techniques that are more efficient or simpler to implement. Nevertheless, it can be concluded that the methods that we have proposed in this article are of sufficiently low time complexity that it would not be a substantial obstacle to implementing them in a practical setting such as in measuring devices.

Future Work

While we have shown that it is possible to identify devices based on the deviation of the discrete cycle length in harmonic emissions, more work would be needed for this method to be a practical alternative for identifying harmonic sources. Some of these are as follows:

- Verify the capture effect with more measurements.

- Evaluate if adaptive filtering is better able to retain useful information when isolating the harmonic under study.
- Evaluate more methods for quantifying the similarity between samples besides the correlation of segments representing the intrinsic periodicity of the signal, perhaps based on machine learning.
- Developing a systematic way of categorising the discrete cycle time behaviour of devices at different operating points.
- Investigate the efficacy of DHCT as a complement for improving the performance of existing methods of harmonic source identification.

Author Contributions: Conceptualisation, T.H. and S.K.R.; methodology, T.H. and S.K.R.; formal analysis, T.H.; resources, S.K.R.; writing—original draft preparation, T.H.; writing—review and editing, T.H. and S.K.R.; visualisation, T.H.; supervision, S.K.R. All authors have read and agreed to the published version of the manuscript.

Funding: This research was funded by the Swedish Transport Administration—Trafikverket.

Data Availability Statement: The raw data supporting the conclusions of this article will be made available by the authors on request.

Acknowledgments: The authors would like to thank Mats Wahlberg and Rafael S. Salles for their help with the laboratory experiments for this study.

Conflicts of Interest: The authors declare no conflicts of interest.

Nomenclature

Sample	the smallest time unit of measurement
Segment	a collection of consecutive samples of a defined length
Epoch	a time series of measurements that is a subset of the entire measurement
Motif	a segment with high similarity to other parts of a time series as identified by matrix profiling
Cycle time	the average time between positive flank zero crossings of a periodic signal
Frequency	the inverse of the cycle time
Instantaneous phase	the phase at each time-step of a sinusoidal signal
Instantaneous frequency (IF)	the time derivative of the instantaneous phase
Instantaneous cycle time	the inverse of IF
Discrete cycle time	the length in time of each discrete cycle

References

1. Bhattacharjee, M.; Prasanna, S.R.M.; Guha, P. Detection of Speech Overlapped with Low-Energy Music using Pyknograms. In Proceedings of the 2021 National Conference on Communications (NCC), Kanpur, India, 27–30 July 2021.
2. Luhn, J.K.; Wright, J.T.; Howard, A.W.; Isaacson, H. Astrophysical Insights into Radial Velocity Jitter from an Analysis of 600 Planet-search Stars. *Astron. J.* **2020**, *159*, 235. [CrossRef]
3. Grigoras, C. Applications of ENF criterion in forensic audio, video, computer and telecommunication analysis. *Forensic Sci. Int.* **2007**, *167*, 136–145. [CrossRef] [PubMed]
4. Safargholi, F.; Malekian, K.; Schufft, W. On the Dominant Harmonic Source Identification-Part I: Review of Methods. *IEEE Trans. Power Deliv.* **2018**, *33*, 1268–1277. [CrossRef]
5. Haili, M.; Girgis, A.A. Identification and tracking of harmonic sources in a power system using a Kalman filter. *IEEE Trans. Power Deliv.* **1996**, *11*, 1659–1665. [CrossRef]
6. D'Antona, G.; Muscas, C.; Sulis, S. Localization of Nonlinear Loads in Electric Systems Through Harmonic Source Estimation. *IEEE Trans. Instrum. Meas.* **2011**, *60*, 3423–3430. [CrossRef]

7. IEC. *International Electrotechnical Vocabulary*; IEC: Geneva, Switzerland, 1990; Available online: https://webstore.iec.ch/publication/181 (accessed on 24 January 2024).
8. *IEC 61000-4-7*; Electromagnetic Compatibility (EMC)—Part 4-7: Testing and Measurement Techniques—General Guide on Harmonics and Interharmonics Measurements and Instrumentation, for Power Supply Systems and Equipment Connected Thereto. IEC: Geneva, Switzerland, 2009.
9. Boashash, B. Estimating and interpreting the instantaneous frequency of a signal. I. Fundamentals. *Proc. IEEE* **1992**, *80*, 520–538. [CrossRef]
10. Huang, N.E. Computing Frequency by Using Generalized Zero-Crossing Applied to Intrinsic Mode Functions. U.S. Patent 6,990,436, 24 January 2006. Available online: https://ntrs.nasa.gov/citations/20080008712 (accessed on 21 February 2024).
11. Fabus, M.S.; Woolrich, M.W.; Warnaby, C.W.; Quinn, A.J. Understanding Harmonic Structures Through Instantaneous Frequency. *IEEE Open J. Signal Process* **2022**, *3*, 320–334. [CrossRef] [PubMed]
12. Huang, N.E.; Shen, Z.; Long, S.R.; Wu, M.C.; Shih, H.H.; Zheng, Q.; Yen, N.-C.; Tung, C.C.; Liu, H.H. The empirical mode decomposition and the Hilbert spectrum for nonlinear and non-stationary time series analysis. *Proc. R. Soc. Lond. Ser. A* **1998**, *454*, 903–995. [CrossRef]
13. Hu, L.; Zhao, B.; Wang, G. A Network Device Identification Method Based on Packet Temporal Features and Machine Learning. *Appl. Sci.* **2024**, *14*, 7954. [CrossRef]
14. Dewesoft. *SIRIUS® Modular Technical Specifications*; Dewesoft: Whitehouse, OH, USA, 2024; Available online: https://dewesoft.com/products/sirius/tech-specs#hs-amplifiers (accessed on 10 February 2025).
15. Pearson Electronics. *Technical Specification: Pearson Current Monitor Model 4100C*; Pearson Electronics: Palo Alto, CA, USA, 2005.
16. Chroma ATE. *Technical Specification: PROGRAMMABLE AC POWER SOURCE*; Chroma ATE: Taoyuan City, Taiwan, 2023; Available online: https://www.chromaate.com/downloads/catalogue/Power/61500-EN.pdf (accessed on 7 September 2024).
17. IEC. *International Electrotechnical Vocabulary (IEV)*; IEC: Geneva, Switzerland, 1992; Available online: https://webstore.iec.ch/publication/239 (accessed on 24 January 2024).
18. Schafer, R.W. On the frequency-domain properties of Savitzky-Golay filters. In Proceedings of the 2011 Digital Signal Processing and Signal Processing Education Meeting (DSP/SPE), Sedona, AZ, USA, 4–7 January 2011.
19. Schmid, M.; Rath, D.; Diebold, U. Why and How Savitzky-Golay Filters Should Be Replaced. *ACS Meas. Sci. Au* **2022**, *2*, 185–196. [CrossRef] [PubMed]
20. Chen, Z.; Li, Z. Robust Precise Time Difference Estimation Based on Digital Zero-Crossing Detection Algorithm. *IEEE Trans. Instrum. Meas.* **2016**, *65*, 1739–1748. [CrossRef]
21. Zero-Crossing Rate—MATLAB Zerocrossrate. The MathWorks, Inc. Available online: https://se.mathworks.com/help/signal/ref/zerocrossrate.html (accessed on 29 January 2024).
22. Interactive Matrix Profile Ver 3.00. University of California, Riverside. 2018. Available online: https://www.cs.ucr.edu/~eamonn/MatrixProfile.html (accessed on 7 September 2024).
23. Linardi, M.; Zhu, Y.; Palpanas, T.; Keogh, E. Matrix profile goes MAD: Variable-length motif and discord discovery in data series. *Data Min. Knowl. Discov.* **2020**, *34*, 1022–1071. [CrossRef]
24. Box-Steffensmeier, J.M.; Freeman, J.R.; Hitt, M.P.; Pevehouse, J.C.W. *Time Series Analysis for the Social Sciences*; Cambridge University Press (CUP): Cambridge, UK, 2014. [CrossRef]
25. Gutiérrez Ballesteros, E.; Gil de Castro, A.; Rönnberg, S.; Sakar, S. Temperature and voltage distortion analysis in LED lamps. *In Proceedings of CIRED* **2019**, *Spain*, 2019. [CrossRef]
26. Stanescu, D.; Enache, F.; Popescu, F. Smart Non-Intrusive Appliance Load-Monitoring System Based on Phase Diagram Analysis. *Smart Cities* **2024**, *7*, 1936–1949. [CrossRef]
27. Wang, Y.-H.; Yeh, C.-H.; Young, H.-W.V.; Hu, K.; Lo, M.-T. On the computational complexity of the empirical mode decomposition algorithm. *Phys. A Stat. Mech. Its Appl.* **2014**, *400*, 159–167. [CrossRef]
28. Li, L. A new complexity bound for the least-squares problem. *Comput. Math. Appl.* **1996**, *31*, 15–16. [CrossRef]
29. Ulloa-Vásquez, F.; Heredia-Figueroa, V.; Espinoza-Iriarte, C.; Tobar-Ríos, J.; Aguayo-Reyes, F.; Carrizo, D.; García-Santander, L. Model for Identification of Electrical Appliance and Determination of Patterns Using High-Resolution Wireless Sensor NETWORK for the Efficient Home Energy Consumption Based on Deep Learning. *Energies* **2024**, *17*, 1452. [CrossRef]

Disclaimer/Publisher's Note: The statements, opinions and data contained in all publications are solely those of the individual author(s) and contributor(s) and not of MDPI and/or the editor(s). MDPI and/or the editor(s) disclaim responsibility for any injury to people or property resulting from any ideas, methods, instructions or products referred to in the content.